Available online at www.sciencedirect.com
SCIENCE DIRECT®
ELSEVIER
European Journal of Mechanics B/Fluids 23 (2004) 241–253
EUROPEAN JOURNAL OF MECHANICS B/FLUIDS

The stability of the boundary layer on a sphere rotating in a uniform axial flow

S.J. Garrett [a], N. Peake [b,*]

[a] *Department of Engineering, University of Cambridge, Trumpington Street, Cambridge CB2 1PZ, UK*
[b] *Department of Applied Mathematics and Theoretical Physics, University of Cambridge, Centre for Mathematical Sciences, Wilberforce Road, Cambridge CB3 0WA, UK*

Received 15 August 2002; received in revised form 18 April 2003; accepted 25 August 2003

Abstract

We consider the local convective and absolute instabilities of the boundary layer on a rotating sphere located in a uniform axial flow, extending our previous work, which considered still outer fluid. Axial flow is seen to stabilise the convective instabilities, and our predicted onset of the spiral vortices is in good agreement with existing experimental data. The vortex angle is found to increase at each latitude with increased axial flow, as does the number of vortices. Results are presented that indicate that the latitude at which "slow" vortices first replace stationary vortices is slightly increased with axial flow. The results of our absolute instability analysis show that axial flow delays the onset of absolute instability at each latitude, and the maximum absolute growth rates are found to reduce with increased axial flow. The onset of absolute instability is found to be much more sensitive to axial flow than is the onset of convective instabilities.

Keywords: Boundary layer; Absolute instability; Rotating sphere

1. Introduction

In this paper the stability of the boundary layer on the surface of a sphere rotating in a uniform axial flow is considered, as an extension of the paper Garrett and Peake [1], in which a sphere rotating in an otherwise still fluid is considered. For the still fluid, convective stability analyses have been conducted by Taniguchi et al. [2] and Garrett and Peake [1]. Garrett and Peake's results extended those of Taniguchi et al. by showing that the characteristics of the spiral vortices tend to those of the rotating disk (Malik [3]) as the rotation rate is increased and the transition region moves towards the pole. Predictions of the vortex speed relative to the sphere surface were also made in [1], and the experimental observation by Kobayashi and Arai [4] of vortices with two distinct speeds (one set "stationary" at moderate latitudes, rotating at the same speed as the sphere, and a second "slow" set, observed only at high latitudes, rotating slower than the sphere) was clarified. Garrett and Peake also conducted local absolute instability analyses at various locations between the pole and the equator. At all latitudes below 70° from the pole, latitudinal absolute instability was found to occur at approximately the same local Reynolds number, with a value close to that found by Lingwood [5,6] on the rotating disk. The predicted onset of absolute instability on the sphere was found to be reasonably close to the experimentally measured onset of turbulence as measured by Kohama and Kobayashi [7] at latitudes below 70°. From these comparisons it was suggested that a latitudinal absolute instability promotes the non-linearity necessary for the onset of turbulence.

* Corresponding author.
E-mail address: n.peake@damtp.cam.ac.uk (N. Peake).

0997-7546/$ – see front matter
doi:10.1016/j.euromechflu.2003.08.004

Rather little theoretical work exists in the literature on the boundary layer of a sphere rotating in a uniform axial flow. El-Shaarawi et al. [8] developed a finite-difference scheme to solve the equations governing the steady laminar boundary-layer flow, but it appears that no stability analyses exist for the problem. Similarly, the problem has received little experimental attention. A number of authors [9–12] have looked at the mass transfer to a rotating sphere in a uniform axial flow, and Luthander and Rydberg [13] have measured the drag induced by the sphere as the axial flow rate is increased. El-Shaarawi et al. [14] have made measurements of the velocity components in the boundary layer and also the separation point as the axial flow rate is increased. More relevant to this present work are the experiments of Kobayashi et al. [15] and Kobayashi and Arai [4]. These papers present details of the spiral vortex behaviour in the transition region of the boundary layer under various rotation and axial flow rates. Their results show that as the axial flow rate is increased a faster rotation rate is required to observe laminar-turbulent transition at each latitude, i.e., axial flow has the effect of stabilising the boundary layer. Unfortunately, unlike the investigation in [7] on the sphere rotating in still fluid, these papers provide no details of the number of vortices or their orientation. However, Kobayashi and Arai do report that the changeover between the stationary and slow vortices is delayed with axial flow, i.e., a larger rotation rate is required for the changeover as the axial flow increases. No measurements are made for the onset of turbulence for varying axial flow rates.

This paper is organised as follows. In Section 2 the solution of the steady boundary-layer equations that give the laminar flow profiles is described, and the unsteady perturbation equations for the system are discussed. The convective and absolute instability analyses are conducted in Sections 3 and 4 respectively, where our theoretical predictions are compared with the limited existing experimental results.

2. Formulation

A sphere of radius $a^\star$ (asterisks indicate dimensional quantities) rotates at constant angular frequency $\Omega^\star$ in a uniform axial flow with free-stream velocity $U^\star_\infty$. Spherical polar coordinates, fixed in space and with origin located at the centre of the sphere, are chosen, with $r^\star$ the radial coordinate, θ the latitude measured from the axis of rotation and ϕ the angle of azimuth. At the edge of the boundary layer the dimensional latitudinal surface velocity distribution (i.e., the slip velocity) is $U^\star_\circ(\theta)$, which is related to the pressure, $P^\star(\theta)$, by the θ-momentum equation

$$\frac{U^\star_\circ}{a^\star}\frac{\partial U^\star_\circ}{\partial\theta} = -\frac{1}{a^\star\rho^\star}\frac{\partial P^\star}{\partial\theta}. \tag{1}$$

The form of the surface velocity distribution $U^\star_\circ$ will be discussed later in this section. The coefficient of kinematic viscosity is denoted by $\nu^\star$ and the density by $\rho^\star$.

The formulation of the problem is very similar to that used in [1]. The slip velocity $U^\star_\circ$ is non-dimensionalized on the free-stream velocity $U^\star_\infty$, while other steady velocities are non-dimensionalized using $\Omega^\star a^\star$. The non-dimensional components of the mean flow in the θ, ϕ and $r^\star$ directions are then

$$U(\eta,\theta) = \frac{U^\star}{\Omega^\star a^\star}, \qquad V(\eta,\theta) = \frac{V^\star}{\Omega^\star a^\star}, \qquad W(\eta,\theta) = \frac{W^\star}{(\nu^\star\Omega^\star)^{1/2}}, \tag{2}$$

respectively. Here $\eta = (\Omega^\star/\nu^\star)^{1/2}(r^\star - a^\star)$ is the radial distance from the sphere surface scaled on the characteristic boundary-layer thickness $\delta^\star = (\nu^\star/\Omega^\star)^{1/2}$.

The equations that govern the mean flow in the boundary layer are stated by Mangler [16] and are non-dimensionalized using (2) as

$$U\frac{\partial U}{\partial\theta} + W\frac{\partial U}{\partial\eta} - V^2\cot\theta = T^2 U_\circ\frac{dU_\circ}{d\theta} + \frac{\partial^2 U}{\partial\eta^2}, \tag{3}$$

$$U\frac{\partial V}{\partial\theta} + W\frac{\partial V}{\partial\eta} + UV\cot\theta = \frac{\partial^2 V}{\partial\eta^2}, \tag{4}$$

$$\frac{\partial W}{\partial\eta} + U\cot\theta + \frac{\partial U}{\partial\theta} = 0, \tag{5}$$

where $T = U^\star_\infty/a^\star\Omega^\star$ is the non-dimensional axial flow parameter, being the ratio of the free-stream flow speed to the speed of the points on the sphere equator. These equations are based on the usual boundary-layer assumption of large Reynolds number.

This choice of scalings will lead to the axial flow parameter T appearing in the basic flow equations only, and the unsteady perturbation equations are identical to those given in [1]. This formulation means that the effect of non-zero axial flow is simply to change the basic flow profiles upon which the stability analyses are performed. We can then look at the relatively small axial

flow rates that are realistically attainable in experiments, perhaps $T < 0.25$, which approach the limit of zero axial flow $T = 0$ studied in [1].

Using (2) the non-slip boundary condition on the surface of the sphere non-dimensionalizes to

$$U = W = V - \sin\theta = 0 \quad \text{on } \eta = 0, \tag{6}$$

and the condition at the edge of the boundary layer becomes

$$V = U - TU_\circ = 0 \quad \text{as } \eta \to \infty. \tag{7}$$

With $T = 0$ the boundary-layer equations (3)–(5) and the boundary conditions (6) and (7) reduce to their zero-axial-flow equivalents given in [1].

We now return to the choice of the surface velocity distribution $U_\circ$. In potential flow the slip velocity distribution is given by

$$U_\circ(\theta) = \frac{3}{2}\sin\theta.$$

However, this inviscid solution is not a good approximation, due to the boundary-layer separation from the sphere surface. A more realistic scaled velocity distribution, as measured by Fage [17], fits the curve

$$U_\circ(\theta) \approx 1.5\theta_{\text{rad}} - 0.4371\theta_{\text{rad}}^3 + 0.1481\theta_{\text{rad}}^5 - 0.0423\theta_{\text{rad}}^7, \tag{8}$$

for $0 \leqslant \theta \leqslant 85^\circ$, and θ_{rad} denotes θ to be measured in radians. This empirical velocity distribution reaches a maximum of $U_\circ = 1.274$ at $\theta = 74^\circ$, whereas the potential-flow distribution reaches a maximum of $U_\circ = 1.5$ at $\theta = 90^\circ$. We have chosen to use the empirical velocity distribution (8) throughout this investigation.

Non-dimensionalizing the relation (1) at the edge of the boundary layer leads to

$$\frac{\partial P}{\partial\theta} = -T^2 U_\circ \frac{\mathrm{d}U_\circ}{\mathrm{d}\theta}, \tag{9}$$

where we have scaled the dimensional pressure as $P^\star = \rho^\star(a^\star\Omega^\star)^2 P$. Using the empirical velocity distribution, $\mathrm{d}U_\circ/\mathrm{d}\theta > 0$ for $\theta < 74^\circ$, and substituting this in (9) shows that

$$\frac{\partial P}{\partial\theta} < 0 \quad \text{for } \theta < 74^\circ.$$

Therefore, at latitudes below $\theta = 74^\circ$ increasing the axial flow rate gives rise to a favourable pressure gradient in the boundary layer, and so is expected to have a stabilizing effect compared to the zero axial flow case.

The solution of (3)–(5) subject to conditions (6) and (7) follows almost exactly the method described in [1] for zero axial flow. One modification that is required is to the initial solution used to initiate marching in the θ direction. The series solution method of Banks [18] is used to approximate the flow at, say, $\theta = 5^\circ$, and the details are broadly as given by [18], except now we have extra terms at each order in the expansion of (3) which arise from the non-zero pressure term in that equation. Figs. 1–3 show the basic velocities U, V and W respectively. Although not shown here, the velocity profiles at latitudes between these show a smooth continuation from the $\theta = 10^\circ$ profile to the $\theta = 70^\circ$ profile as the latitude is increased.

In Fig. 3 we see W tending to a constant gradient as $\eta \to \infty$, as is to be expected in an accelerating boundary layer. The gradient increases with T, and can be calculated from (5) using condition (7), i.e.,

$$\frac{\partial W}{\partial\eta} \sim -T\left(U_\circ\cot\theta + \frac{\partial U_\circ}{\partial\theta}\right).$$

Physically, this behaviour cannot be maintained arbitrarily far from the surface, as it predicts that fluid is entrained into the boundary layer with unbounded speed as the radial distance is increased, and is of course a consequence of the boundary-layer approximations. The paper by El-Shaarawi et al. [14] shows experimental measurements of these velocity components, and measured W-profiles do indeed behave as in Fig. 3 in the boundary layer. Very close to the sphere surface, Figs. 1–3 show that the flow is independent of the axial flow rate.

In the analysis presented here the boundary layer is approximated by the region $0 \leqslant \eta \leqslant 20$ and so the W-profiles used are those shown in Fig. 3. It is important to note that the region is sufficiently large for the velocity components U and V to be fully developed. In the governing equations, W is scaled by the Reynolds number, which is necessarily large in the boundary-layer approximation, so that the cramping of the boundary layer should not cause major inaccuracies. In any event, different computational boundary-layer thicknesses were tested in order to check that an outer boundary of $\eta = 20$ did indeed give converged unsteady flow results.

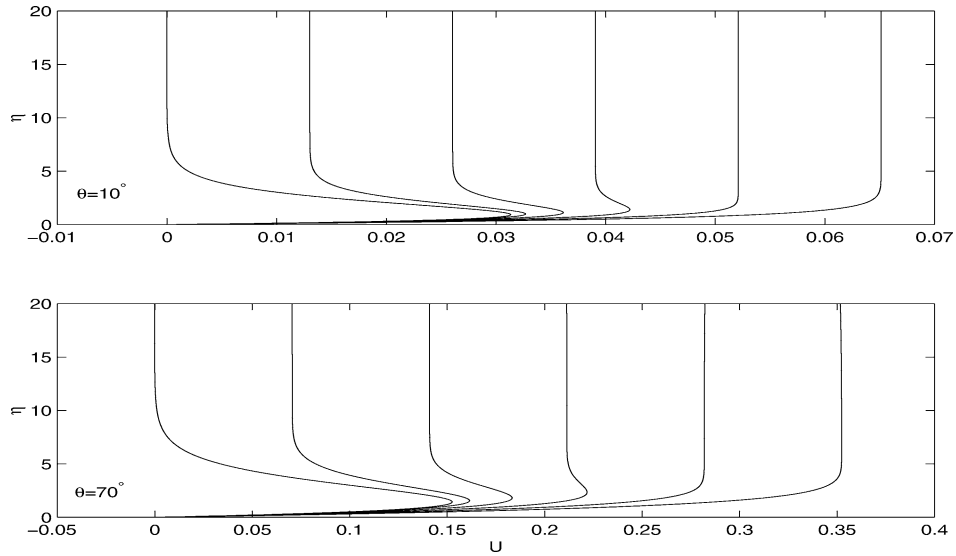

Fig. 1. The latitudinal velocity U at $\theta = 10°$ and $70°$ with $T = 0.00 \to 0.25$ in 0.05 increments (left to right).

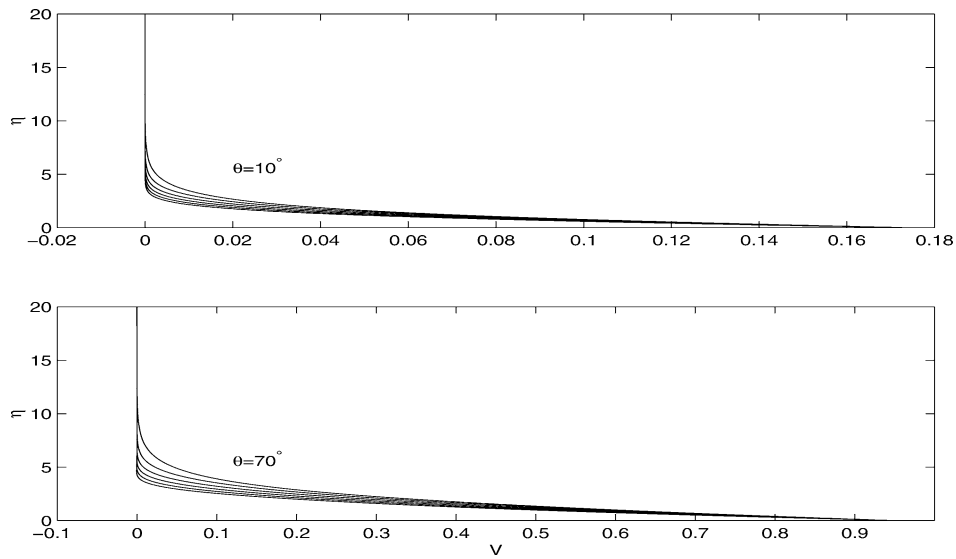

Fig. 2. The azimuthal velocity V at $\theta = 10°$ and $70°$ with $T = 0.00 \to 0.25$ in 0.05 increments (top to bottom).

We impose infinitesimally small perturbations (denoted by lower case hatted quantities) on the steady mean flow in the boundary layer at a given latitude, in the dimensional form

$$(\hat{u}^\star, \hat{v}^\star, \hat{w}^\star, \hat{p}^\star) = \left(u^\star(r^\star), v^\star(r^\star), w^\star(r^\star), p^\star(r^\star)\right) \mathrm{e}^{\mathrm{i}(\alpha^\star a^\star \theta + \beta^\star a^\star \phi \sin\theta - \gamma^\star t^\star)}. \tag{10}$$

These perturbations are non-dimensionalized on the typical length, velocity, time and pressure scales: $\delta^\star$, $a^\star\Omega^\star$, $\delta^\star/a^\star\Omega^\star$ and $\rho^\star(a^\star\Omega^\star)^2$ respectively. The mean-flow quantities are non-dimensionalized as in (2), which leads to the Reynolds number $R = \delta^\star a^\star \Omega^\star/\nu^\star = a^\star/\delta^\star$.

As mentioned before, the formulation of this problem is such that the axial flow, T, appears only in the steady-flow equation (3) and the boundary condition (7). For this reason the relevant unsteady perturbation equations are identical to those of [1] and are given by Eqs. (2.13)–(2.18) of that paper, and in the Appendix here for completeness. Details of the derivation of the perturbation equations can be found in [1], which includes a discussion of the parallel-flow approximation made. Here it is sufficient to note that the parallel-flow approximation limits the analysis to a local analysis at each value of θ.

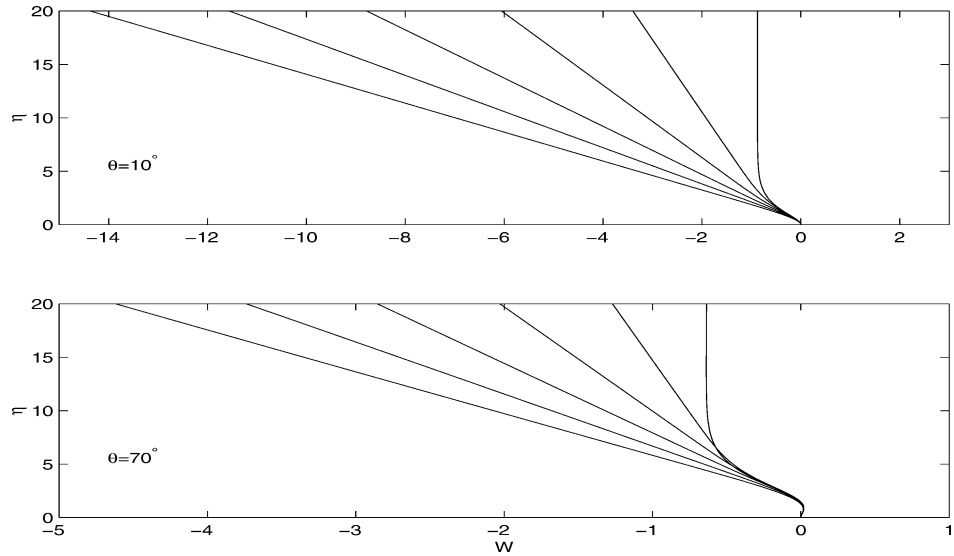

Fig. 3. The radial velocity W at $\theta = 10°$ and $70°$ with $T = 0.00 \to 0.25$ in 0.05 increments (right to left).

In our subsequent spatio–temporal analysis we will require the θ wavenumber, α, and frequency, ω, to be complex. However, in order to enforce periodicity around the azimuth we will require the azimuthal wavenumber, β, to be real, with $\beta = n/R\sin\theta$ for integer n. We will identify n as being the number of spiral vortices on the sphere surface, which make an angle ε to the equator, with

$$\varepsilon = \tan^{-1}(\beta/\alpha_r). \tag{11}$$

3. Convective instability

We now solve the homogeneous eigenvalue problem defined by the unsteady perturbation equations in [1], to describe the local dispersion relation at each θ and for given T. The numerical procedure for doing this is discussed in [1].

In the first instance we suppose that the flow is not absolutely unstable, so that in the Briggs–Bers procedure (Briggs [19], Bers [20]) we can reduce the imaginary part of the frequency down to zero. Two approaches can now be taken. First, in Section 3.1, regions of convective instability are found at each latitude by insisting that the vortices rotate at some fixed multiple, c, of the sphere surface velocity, thereby fixing $\gamma_r = c\beta\sin\theta = cn/R$. For $c = 1.0$ the vortices rotate with the sphere, while Kobayashi and Arai [4] observe slow vortices with $c = 0.76$ at high latitudes. Second, in Section 3.2, individual neutral curves are plotted at each latitude for each n, and the full neutral curve at a particular latitude is then the envelope of theses neutral curves over all n. A prediction of the rotation speed of the spiral vortices can then be made.

3.1. Disturbances with rotation speed $c = 1$

Two spatial branches are found that determine the convective instability characteristics at each latitude for each axial flow rate. These branches arise from crossflow and streamline-curvature instability modes and are identical to those discussed in [1]; for this reason we do not discuss them in detail here. However, we note that the crossflow instability mode arises from the inflectional nature of the latitudinal mean velocity component, U, while the streamline-curvature mode corresponds to a centrifugal instability associated with the way in which the outer-flow streamlines are curved by an $O(R^{-1})$ amount close to the outer edge of the boundary layer.

Fig. 4 shows the neutral curves in the (R, α_r)- and (R, β)-planes at $\theta = 30°$ for each T. The neutral curves are determined by setting $\gamma_i = 0$ (i.e., neutral disturbance), $\beta_i = 0$ (azimuthal periodicity), and $\gamma_r = \beta_r\sin\theta$ (to guarantee $c = 1$) and for each R the dispersion relation is then solved to return a pair of values (α_r, β_r) for each neutral mode. As can be seen in Fig. 4, the value of β varies continuously, although of course for a given value of R only those values of β which give an integer value of n are allowed physically. Inside each loop of the neutral curves the flow is convectively unstable. The two-lobed structure is seen in the neutral curves for each T at all latitudes below $\theta = 60°$ (only $\theta = 30°$ shown here). The larger lobe, characterised by

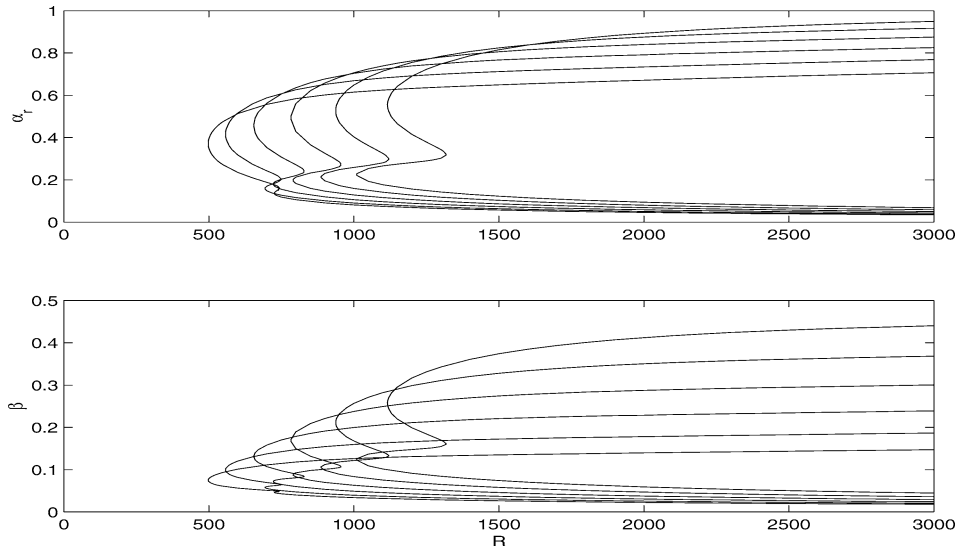

Fig. 4. Neutral curves for the convective instability of stationary vortices at $\theta = 30^\circ$ with $T = 0.00 \rightarrow 0.25$ (left to right) in 0.05 increments.

Table 1
The critical Reynolds number R for the onset of the crossflow mode of convective instability at latitudes $\theta = 10{-}60^\circ$ for axial flow rates $T = 0.05{-}0.25$, – indicates that a crossflow lobe is not seen

T	$\theta = 10^\circ$	$\theta = 20^\circ$	$\theta = 30^\circ$	$\theta = 40^\circ$	$\theta = 50^\circ$	$\theta = 60^\circ$
0.05	1799	872	558	396	293	213
0.1	2118	1026	655	464	348	–
0.15	2526	1225	783	555	418	–
0.2	3050	1462	968	667	514	–
0.25	3543	1731	1116	797	623	–

Table 2
The critical Reynolds number R for the onset of the streamline-curvature mode of convective instability at latitudes $\theta = 10{-}60^\circ$ for axial flow rates $T = 0.05{-}0.25$

T	$\theta = 10^\circ$	$\theta = 20^\circ$	$\theta = 30^\circ$	$\theta = 40^\circ$	$\theta = 50^\circ$	$\theta = 60^\circ$
0.05	2380	1122	694	470	318	197
0.1	2486	1171	723	492	330	201
0.15	2722	1281	791	536	365	225
0.2	3061	1436	887	604	420	263
0.25	3438	1626	1010	691	491	316

higher wave numbers α_r, is due to crossflow instabilities and the smaller lobe, characterised by smaller α_r, is due to streamline-curvature instabilities. At $\theta = 60^\circ$ when $T > 0.05$ and at $\theta = 70^\circ$ for all T, the cusp separating the two lobes is not seen and so these curves are considered to be single-lobed. The single lobe is due to the streamline-curvature instability merging with the crossflow instability which defines the shape of the upper branch. However, these calculations assume stationary vortices ($c = 1.0$), which is not a valid assumption for higher latitudes. For this reason the calculations conducted at $\theta = 70^\circ$ will not be compared with the experimental results of Kobayashi and Arai [4].

Fig. 4 shows that increasing the axial flow rate has the effect of increasing the critical Reynolds number of each instability mode. This is seen at all latitudes, as shown in Tables 1 and 2. The two-lobed structure of the neutral curves is found to be exaggerated by the axial flow when $\theta < 60^\circ$, with the streamline-curvature lobe becoming more important with respect to the crossflow lobe with increased T. At all latitudes below $\theta = 60^\circ$ the streamline-curvature mode becomes the most dangerous mode above a certain value of T, which decreases with increased latitude. The observation that an increased axial flow rate increases the strength of the streamline-curvature mode is sensible, as Fig. 3 shows that axial flow increases the amount of

fluid entrained into the boundary layer, leading to more streamline curvature. Garrett and Peake [1] found that the streamline-curvature mode becomes more important as the latitude is increased, as a consequence of the geometry of the boundary layer on the sphere. This is consistent with the observation that the value of T at which the streamline curvature mode is seen to dominate decreases with latitude.

The lower branch of the neutral curves in Fig. 4 is seen to be independent of T for sufficiently large R at all latitudes. In contrast, the upper branch of each neutral curve depends on the value of T. Increasing T moves the upper branch higher up the wavenumber axis in both parameter planes. This suggests that even though axial flow stabilizes the boundary layer in the sense that it increases the critical Reynolds numbers for each instability mode, axial flow increases the range of wavenumbers over which instability can occur.

Kobayashi and Arai [4] have measured the locations of the onset of spiral vortices on a sphere rotating in a non-zero axial flow, and we now try to associate the appearance of the spiral vortices with the onset of convective instability. The experimental results are expressed in terms of a local Reynolds number Re_l that is based on the local latitudinal flow velocity at the outer edge of the boundary layer and the boundary-layer thickness there. Re_l is related to our Reynolds number by $Re_l = TU_\circ R$ and their axial flow parameter is defined by $S = 3/(2T)$. The critical values of R that were predicted in our analysis have been converted to Re_l at each S and are plotted in Fig. 5. Experimental measurements for the onset of the spiral vortices are also indicted on the figure at three different axial flow rates, and we see fair agreement between our predicted onset of the crossflow mode and the experimental data. The experimental measurements were conducted in [4] on three different sized spheres for each axial flow rate, hence the three experimental points for each S.

Fig. 6 gives the predicted values of the vortex angle, ε, against T at the onset of each instability mode at each latitude. The value of ε at the onset of the crossflow mode is seen to be roughly independent of latitude and increases linearly with T. At the onset of the streamline-curvature mode the predicted value of ε is dependent on both the latitude and axial flow rate. The dependence on latitude sees ε decreasing with increased θ at each T. Again, ε is seen to increase with increased T. Unfortunately, no experimental data appears to exist concerning the orientation of the vortices on a sphere rotating in an axial flow, and the theoretical predictions cannot be compared with experimental data at present.

Fig. 7 gives the predicted values of the vortex number, n, against T at each latitude for the onset of both crossflow and streamline-curvature instability modes. At each latitude, and for both instability mode types, n is predicted to increase with axial flow speed. For each T, n is predicted to increase as we approach the pole, which is consistent with the non-zero axial flow observations. Unfortunately, no experimental data can be found concerning the number of vortices on a sphere rotating in a non-zero axial flow, and again these theoretical predictions cannot be compared with experimental data.

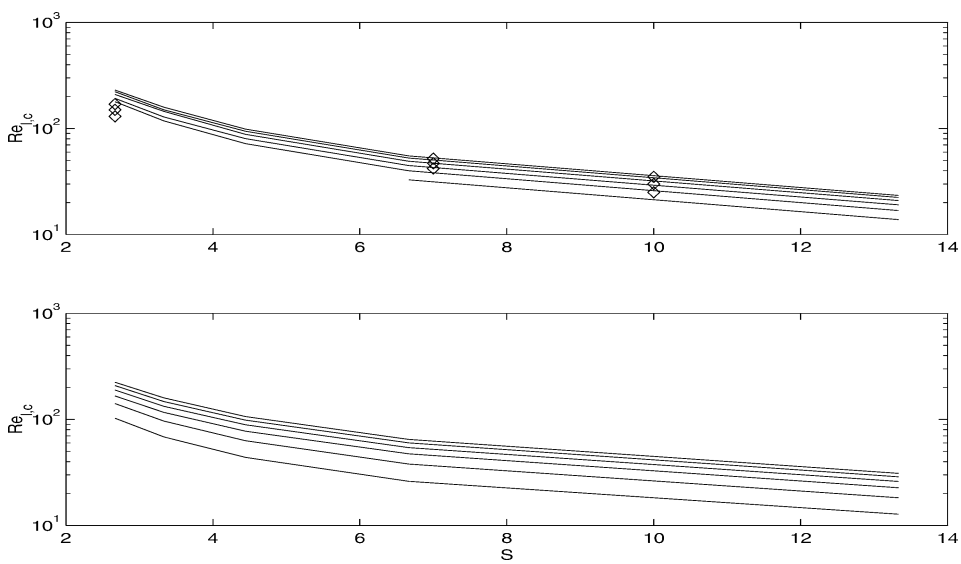

Fig. 5. Plot of the critical local Reynolds numbers ($Re_{l,c}$) for the onset of crossflow (top) and streamline-curvature (bottom) modes at latitudes $\theta = 10^\circ \to 60^\circ$ (top to bottom) in 10° increments. The highlighted points are from experiments conducted by Kobayashi and Arai [4] on three different spheres, each under three different axial flow rates.

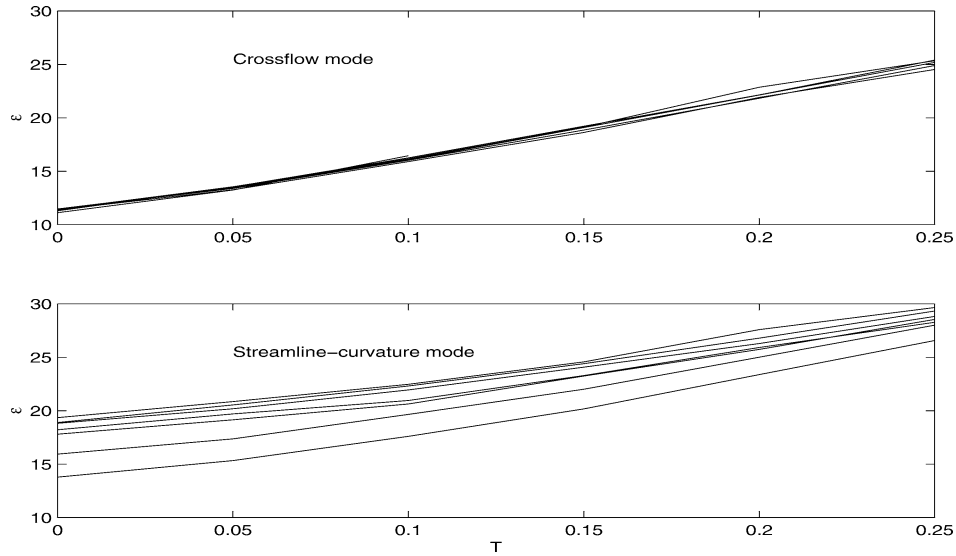

Fig. 6. The vortex angle ε, in degrees, against axial flow rate at the onset of each instability mode type at latitudes of $10^\circ \to 70^\circ$ (top to bottom in the second figure).

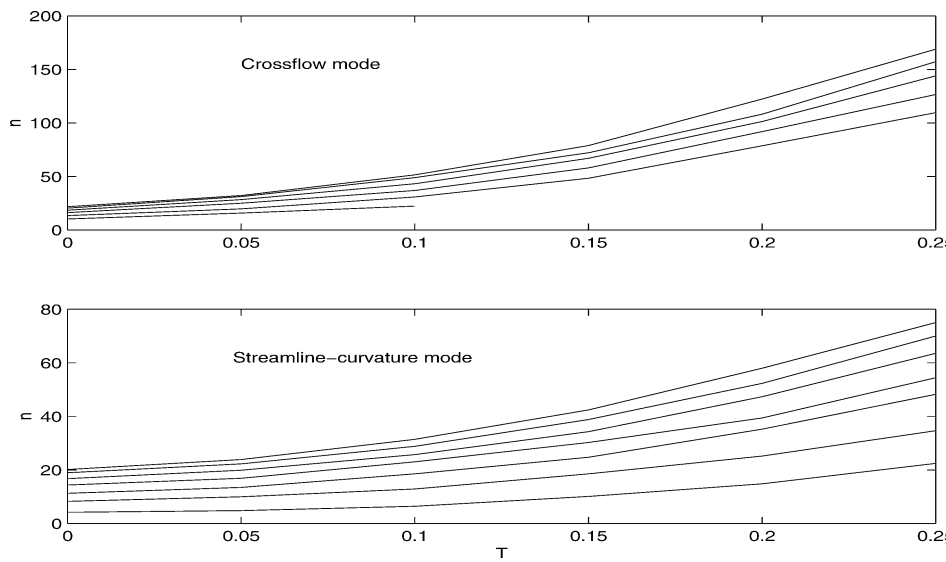

Fig. 7. The number of vortices against axial flow rate at the onset of each instability mode type at latitudes of $10^\circ \to 70^\circ$ (top to bottom).

3.2. Disturbances with rotation speed $c \neq 1$

We now calculate the individual neutral curves $\gamma_i = \alpha_i = 0$ for given n, and then plot the envelope of these curves for all n to give a full neutral curve at a given latitude. In this way, the longitudinal wave speed, c, will be predicted from the critical value of γ_r via $c = \gamma_r R/n$.

Fig. 8(a) shows that at $\theta = 60^\circ$ the curves have a single minimum and, although not shown here, this is the case at all latitudes below $\theta = 60^\circ$ as well. The minimum occurs at the critical Reynolds number of the crossflow lobe of the enveloping neutral curve, and is almost identical to that calculated in Section 3.1, so that the critical values of γ_r and R at the minimum of each curve lead to the prediction that $c \approx 1.0$. Setting $c = 1.0$ at these latitudes for each T, as was done in Section 3.1, is therefore correct.

As the latitude is increased from $\theta = 60^\circ$ the curves flatten out and an inflection point is seen at $\theta = 70^\circ$ when $T < 0.25$, as shown in Fig. 8(b). By looking carefully at latitudes $60^\circ < \theta < 70^\circ$, we have found that when $T = 0.05$ the inflection point first

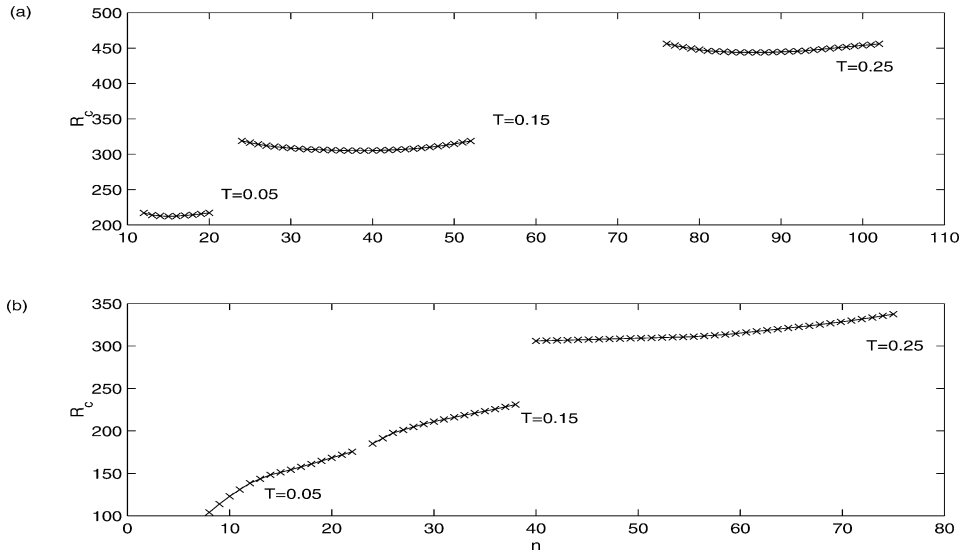

Fig. 8. Critical Reynolds numbers, R_c, at latitudes (a) $\theta = 60°$ and (b) $\theta = 70°$ with axial flow rates $T = 0.05$, 0.15 and 0.25 for neutral curves defined by fixing n at various integer values.

appears at $\theta = 67°$ and when $T = 0.15$ the inflection point first appears at $\theta = 69°$. For $T = 0.25$, Fig. 8(b) shows that the curve is just at the changeover point; at $\theta = 71°$ an inflection point would be found instead of a minimum. Of course, this method does not predict what value of c should actually be taken at high latitudes, it merely predicts that stationary vortices, with $c = 1$, are no longer present. In Fig. 8(b) the critical Reynolds numbers for the smaller values of n (e.g., $n \leqslant 9$ for $T = 0.05$) lie below the range of Reynolds numbers plotted, but we emphasise that the distinct turning points seen in Fig. 8(a) are absent.

The experimental observations of Kobayashi and Arai [4] suggest that the effect of axial flow is to delay the changeover between slow and stationary vortices, i.e., axial flow increases the Reynolds number at which the changeover occurs. Our results are consistent with this observation, and we are also able to predict that the latitude for the changeover increases slightly, from $\theta = 66°$ for $T = 0$ to $\theta = 71°$ for $T = 0.25$. Unfortunately, details of the latitude at which changeover occurs are not given in [4].

Garrett and Peake [1] have shown that in zero axial flow the onset of the slow vortices occurs at $\theta = 66°$. At this latitude a small region of reverse flow occurs in the radial component of the mean flow, and this coincides with the dominance of the streamline-curvature mode. However, for non-zero T we find that although the onset of slow vortices still occurs close to this latitude and reverse flow is still seen here, it does not coincide with the dominance of the streamline-curvature instability mode.

4. Absolute instability

We now solve our eigenvalue problem with the aim of studying the occurrence of absolute instability. The Briggs–Bers method is used to detect absolutely-unstable response to the impulsive line forcing $\delta(\theta - \theta_s)\delta(t)\exp(in\phi)$. For absolute instability to occur, we require a pinch point, $\gamma = \gamma^\circ$, $\alpha^\circ = \alpha(\gamma^\circ)$, formed by the coalescence of branches originating in opposite α half planes for γ_i large and positive. This pinch point is then unstable if $\gamma_i^\circ > 0$.

Pinch-points with $\gamma_i^\circ > 0$ have been found at all latitudes for each axial flow rate, and so the boundary layer on the sphere rotating in a uniform axial flow is absolutely unstable for certain values of R and β, which depend on T, at each latitude. The neutral curves for absolute instability at each latitude are of a similar shape to those calculated in [1], and for this reason they are not shown here. The critical Reynolds numbers for the onset of absolute instability at each latitude are shown in Table 3 for axial flow rates between $T = 0.05$ and 0.25 (and for comparison for $T = 0$ taken from Table 1 of [1]). These results show that axial flow has the effect of stabilising the boundary layer to absolute instabilities at each latitude, i.e., the critical Reynolds numbers are increased with increased T at each θ. The critical Reynolds numbers increase a great deal with increased axial flow, and much more than the critical Reynolds numbers for the onset of convective instability. For example, at $\theta = 30°$, the critical Reynolds number for the onset of absolute instability increases by a factor greater than 20 between $T = 0.05$ and $T = 0.25$, while in contrast the critical Reynolds number for the onset of convective instability increases only by a factor of 2. We do not have a physical explanation at present for why the absolute instability results are far more sensitive to changes in the value of the axial flow.

Table 3
The critical Reynolds number R for the onset of absolute instability at each latitude θ and axial flow rate T

T	$\theta = 10°$	$\theta = 20°$	$\theta = 30°$	$\theta = 40°$	$\theta = 50°$	$\theta = 60°$	$\theta = 70°$
0	2880	1413	912	650	480	352	240
0.05	4192	2053	1321	939	709	519	344
0.1	7404	3602	2298	1626	1270	937	624
0.15	15264	7355	4627	3242	2666	1998	1365
0.2	44254	17355	10739	7564	6544	5075	3746
0.25	102301	47855	28981	19971	19138	15809	14194

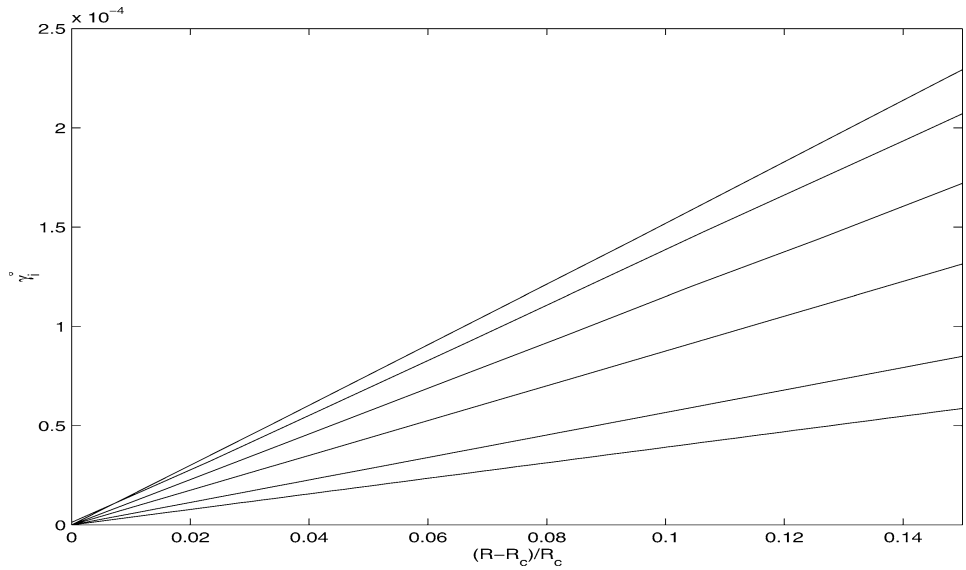

Fig. 9. The behaviour of the maximum growth rates as we move into the region of instability at $\theta = 10°$ for $T = 0.00 \to 0.25$ (top to bottom) in increments of 0.05.

The effect of axial flow on the absolute instability of the boundary layer can also be judged by looking at the behaviour of the absolute growth rates at each latitude as the axial flow rate is increased. More precisely, we can look at how the maximum growth rates behave as we move further into the region of absolute instability of each neutral curve. Fig. 9 shows the maximum absolute growth rates at various points in the region of absolute instability for each T at $\theta = 10°$. The results are qualitatively similar at all latitudes and so it is sufficient to show only this figure. The most important observation to make is that the growth rates reduce with increased axial flow, and tend to zero as T increases, and suggesting that axial flow suppresses the absolute instability within the boundary layer.

For a sphere rotating in an otherwise still fluid, it is shown in [1] that the local Reynolds numbers at the onset of absolute instability are roughly the same at all latitudes below $\theta = 70°$ but have a slight deviation that increases with latitude. Above $\theta = 70°$ the critical local Reynolds number is substantially lower. Fig. 10 shows that this is also true for non-zero axial flow (note that we also include $T = 0$ results for comparison). The local Reynolds number, $R_X = R^2\theta\sin\theta$, is formed using the distance to the latitude in question from the pole over the sphere surface, $a^\star\theta$, as the length scale and the local surface rotation speed at that point, $a^\star\Omega^\star\sin\theta$, for the velocity scale. From Fig. 10 we see that the local Reynolds number at the onset of absolute instability is roughly independent of the latitude for each value of T when close to the pole. The value of this critical local Reynolds number increases with increased T, hence demonstrating the stabilising effect of the axial flow. We also see that the deviation from the constant value near to the pole that occurs as we move up the sphere is accelerated with increased axial flow. The comparisons made in [1] with the experimental data of Kohama and Kobayashi [7] do suggest that if the boundary-layer transition is governed by absolute instability, then it would only be for latitudes where the critical local Reynolds number is approximately independent of latitude. Fig. 10 therefore indicates that if absolute instability does promote transition in the boundary layer then it can only do so in an increasingly limited region close to the pole. However, for this to be correct the critical local Reynolds numbers would need to be sufficiently close to experimental measurements for the onset of turbulence and, unfortunately, it appears that these measurements do not yet exist.

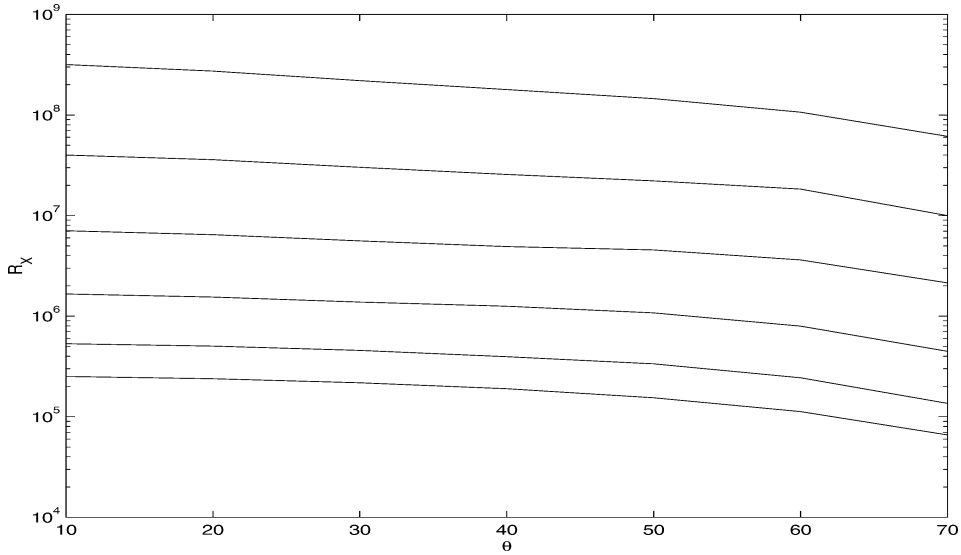

Fig. 10. Predicted critical R_X values for absolute instability for $T = 0.00 \rightarrow 0.25$ in 0.05 increments (bottom to top).

5. Conclusion

In this paper we have followed the formulation of Garrett and Peake [1] by scaling the boundary-layer variables on the boundary-layer thickness and the surface rotation rate at the equator. This formulation allows the introduction of axial flow into the problem by continuously increasing the axial flow parameter $T = U_\infty^\star/(a^\star\Omega^\star)$ from zero. Using this formulation the perturbation equations relevant to the axial flow problem are identical to those in [1]. The effect of non-zero axial flow on the analysis is therefore to change the basic flow profiles upon which the analysis is performed.

For stationary vortices, we have seen that axial flow stabilises the boundary layer with respect to convective instabilities. At all latitudes below $\theta = 60^\circ$ we see reasonable agreement with the predicted onset of the crossflow mode and the measurements of Kobayashi and Arai [4] for the onset of instability.

Kobayashi and Arai's experimental observations suggest that the effect of axial flow is to delay the changeover between slow and stationary vortices, i.e., axial flow increases the Reynolds number at which the changeover occurs. Our predictions of the vortex speed are consistent with this observation, and we were also able to predict that the latitude for the changeover increases slightly from $\theta = 66^\circ$ for $T = 0$ to $\theta = 71^\circ$ for $T = 0.25$.

We have also seen that axial flow stabilises the boundary layer to absolute instability. This was shown by the critical Reynolds numbers increasing with axial flow at each latitude, and also by the maximum absolute growth rates being reduced at each latitude with increased axial flow. At each axial flow rate the onset of absolute instability is seen to occur at a roughly constant value of the local Reynolds number as we move away from the pole. This behaviour was also found in [1] for a sphere rotating in an otherwise still fluid. However, the deviation from this constant value as we move away from the pole is accelerated with increased axial flow.

Of course, all the results presented in this paper depend on the precise form of the outer slip velocity which is adopted. We have also performed calculations with the simple potential slip velocity, $(3/2)\sin\theta$, and found qualitative agreement with the results from the Fage slip distribution. Quantitatively, both slip distributions give very similar convective and absolute critical Reynolds numbers for $\theta \leqslant 40^\circ$, but discrepancies arise at larger angles close to the Fage point of maximum slip velocity ($\theta = 74^\circ$). Of course, the Fage distribution is a much better representation of the real flow, and has therefore been used throughout this paper.

A number of other open issues remain, requiring experimental clarification and validation, including the vortex angle and number, and also the location of the changeover to slow vortices as a function of the axial flow rate. Additional effects could also be included in our analysis, such as the behaviour of more general bodies of revolution.

Results presented here have been taken from purely local stability calculations, and therefore do not take proper account of non-parallel effects associated with variations in the boundary layer with θ. However, the authors have attempted to search for linear global modes on the sphere (in zero axial flow) [21], by extending strictly inviscid locally absolute frequencies into the complex θ plane and seeking resonant behaviour. A neutral global mode has indeed been identified, at least for sufficiently high rotation rates of a given sphere.

Acknowledgement

SJG was supported by the Engineering and Physical Sciences Research Council and the Newton Trust of Cambridge University.

Appendix A. The perturbation equations

The perturbation equations can be written as a set of six first-order ordinary differential equations in the form

$$Dz_1 = z_2, \tag{A.1}$$

$$\begin{aligned}\left[\frac{Dz_2}{R}\right]_v = {} & \frac{1}{R}\left(\left[\alpha^2+\beta^2\right]_v + \mathrm{i}R(\alpha U+\beta V-\gamma)\right)z_1 + \left[\frac{Wz_2}{R}\right]_s + \left(\alpha_1 U' + \beta V' + \left[\frac{1}{R}(\alpha_1 U+\beta V)\right]_s\right)z_3 \\ & + \mathrm{i}\left(\left[\alpha^2+\beta^2\right]_v - \left[\frac{\mathrm{i}\alpha\cot\theta}{R}\right]_s\right)z_4 - \left[\frac{V\cot\theta z_5}{R}\right]_s \\ & + \left[\frac{1}{R}\left(\left(\alpha_1\frac{\partial U}{\partial\theta}+\beta\frac{\partial V}{\partial\theta}\right)u - (\alpha_1 V-\beta U)v\cot\theta\right)\right]_s,\end{aligned} \tag{A.2}$$

$$Dz_3 = -\mathrm{i}\phi_1 - \left[\frac{2z_3}{R}\right]_s, \tag{A.3}$$

$$Dz_4 = \left[\frac{\mathrm{i}Wz_1}{R}\right]_s - \left[\frac{\mathrm{i}z_2}{R}\right]_v + \left[\frac{2}{R}(Uu+Vv)\right]_s - \frac{1}{R}\left(\left[\alpha^2+\beta^2\right]_v + \mathrm{i}R(\alpha U+\beta V-\gamma) + DW_s\right)z_3, \tag{A.4}$$

$$Dz_5 = z_6, \tag{A.5}$$

$$\begin{aligned}\left[\frac{Dz_6}{R}\right]_v = {} & \left[\frac{V\cot\theta z_1}{R}\right]_s + \left(\alpha_1 V' - \beta U' + \left[\frac{1}{R}(\alpha_1 V-\beta U)\right]_s\right)z_3 \\ & + \left[\frac{Wz_6}{R}\right]_s + \left[\frac{1}{R}\left(\left(\alpha_1\frac{\partial V}{\partial\theta}-\beta\frac{\partial U}{\partial\theta}\right)u + (\alpha_1 U+\beta V)v\cot\theta\right)\right]_s \\ & + \left[\frac{\beta\cot\theta z_4}{R}\right]_s + \frac{1}{R}\left(\left[\alpha^2+\beta^2\right]_v + \mathrm{i}R(\alpha U+\beta V-\gamma)\right)z_5,\end{aligned} \tag{A.6}$$

where

$$z_1 = (\alpha - \mathrm{i}\cot\theta/R)u + \beta v, \qquad z_2 = (\alpha - \mathrm{i}\cot\theta/R)Du + \beta Dv, \qquad z_3 = w,$$
$$z_4 = p, \qquad z_5 = (\alpha - \mathrm{i}\cot\theta/R)v - \beta u, \qquad z_6 = (\alpha - \mathrm{i}\cot\theta/R)Dv - \beta Du, \qquad \alpha_1 = \alpha - [\mathrm{i}\cot\theta/R]_s,$$

D represents differentiation with respect to η and the subscripts v and s indicate which of the $\mathrm{O}(R^{-1})$ terms arise from the viscous and streamline-curvature effects respectively.

References

[1] S.J. Garrett, N. Peake, The stability and transition of the boundary layer on a rotating sphere, J. Fluid Mech. 456 (2002) 199–218.
[2] H. Taniguchi, T. Kobayashi, Y. Fukunishi, Stability of the boundary layer on a sphere rotating in still fluid, Acta Mech. 129 (1998) 243–253.
[3] M.R. Malik, The neutral curve for stationary disturbances in rotating-disk flow, J. Fluid Mech. 164 (1986) 275–287.
[4] R. Kobayashi, T. Arai, Spiral vortex behaviour in transition region and separation of three-dimensional boundary layers on spheres rotating in axial flow, in: D. Arnal, R. Michel (Eds.), Laminar Turbulent Transition, IUTAM Symposium Toulouse, France, Springer-Verlag, Berlin, 1990, pp. 551–557.
[5] R.J. Lingwood, Absolute instability of the boundary layer on a rotating disk, J. Fluid Mech. 299 (1995) 17–33.
[6] R.J. Lingwood, An experimental study of absolute instability of the rotating-disk boundary-layer flow, J. Fluid Mech. 314 (1996) 373–405.
[7] Y. Kohama, R. Kobayashi, Boundary-layer transition and the behaviour of spiral vortices on rotating spheres, J. Fluid Mech. 137 (1983) 153–164.
[8] M.A.I. El-Shaarawi, M.F. El-Refaie, S.A. El-Bedeawi, Numerical solution of laminar boundary layer flow about a rotating sphere in an axial stream, Trans. ASME, J. Fluids Engrg. 107 (1985) 97–104.

[9] P. Noordzij, J.W. Rotte, Mass transfer coefficients to a rotating and to a vibrating sphere, Chem. Engrg. Sci. 22 (1967) 1475.
[10] P. Noordzij, J.W. Rotte, Mass transfer coefficient for simultaneously rotating and translating sphere, Chem. Engrg. Sci. 23 (1968) 657.
[11] T. Furuta, T. Jimbo, M. Okazaki, R. Toei, Mass transfer to a rotating sphere in an axial stream, J. Chem. Engrg. Japan 8 (1975) 457.
[12] H. Tanaka, O. Tago, Mass transfer from a rotating sphere in air stream, Kagaku Kögaku 37 (1975) 151.
[13] S. Luthander, A. Rydberg, Experimentelle untersuchungen über den luftwiderstand bei einer um eine mit der windrichtung parallelen achse rotieren kugel, Phys. Z. 36 (1935) 552–558.
[14] M.A.I. El-Shaarawi, M.M. Kemry, S.A. El-Bedeawi, Experiments on laminar flow about a rotating sphere in an air sphere, Proc. Inst. Mech. Engrg. 201 (C6) (1987) 427–438.
[15] R. Kobayashi, T. Arai, M. Nakajima, Boundary layer transition and separation on spheres rotating in axial flow, Exp. Thermal Fluid Sci. 1 (1980) 99–104.
[16] W. Mangler, Boundary layers on bodies of revolution in symmetrical flow, Ber. Aerodyn Versuchsanst. Goett, Report 45/A/17, 1945.
[17] A. Fage, Experiments on a sphere at critical Reynolds numbers, Aero. Res. Council London, R & M 1766 (1936).
[18] W.H.H. Banks, The boundary layer on a rotating sphere, Q. J. Mech. Appl. Math. 18 (1965) 443–454.
[19] R.J. Briggs, Electron-Stream Interaction with Plasmas, MIT Press, 1964.
[20] A. Bers, Linear waves and instabilities, in: C. DeWitt, J. Peyraud (Eds.), Physique des Plasmas, Gordon and Breach, 1975, pp. 117–215.
[21] S.J. Garrett, The stability and transition of the boundary layer on rotating bodies, Ph.D. Thesis, University of Cambridge.